Review article

Understanding Mass Transport Influenced Electrocatalysis at the Nanoscale via Numerical Simulation

Chuhong Lin and Richard G. Compton*

Department of Chemistry, Physical and Theoretical Chemistry Laboratory, Oxford University, South Parks Road, Oxford OX1 3QZ, UK.

* Corresponding author, E-mail: richard.compton@chem.ox.ac.uk.

Abstract

Electrochemical responses reflect both electron transfer and mass transport. Unscrambling electrocatalytic effects requires the quantitative separation of the two. This needs simulation to permit modelling of voltammograms and other data. We survey the key principles and show how authentic effects can be identified with confidence.

Keywords

Electrocatalysis, Mass transport, Nanoelectrode, Simulation, Nanoeffect

1 Introduction

Electrocatalysis using nano-sized entities is of significant interest in both fundamental kinetic studies and for potential practical applications. The development of nanoelectrodes together with nanocell fabrication, scanning electrochemical microscopy and the nanoparticle collision technique makes it possible to observe electrocatalysis at single nanoentities.[1-5] Synergy with numerical simulation provides crucial informative understanding and insight.

For heterogeneous catalysis at the micro- or nano-scale, competition in kinetics between mass transport and reaction is a primary factor. The influence of mass transport on nanoscale heterogeneous catalysis arises because of the comparability of length scales between the effective catalyst radius and the size of the reaction region where the reactant concentration or the electric potential is different from that in the bulk solution.[6] This short review mainly focuses on diffusion when discussing the "mass transport influence" on convection free electrochemical systems, mostly but not exclusively (see Section 2.3) under highly supported electrolyte conditions. In particular the comparability in rates between diffusion and electrochemical reaction needs to be explored and quantified for electrocatalysis at single nanoentities.

In this review, recent studies on the electrocatalytic kinetics of nanoelectrodes and nanoparticles are overviewed; the mass transport influence and the role of numerical simulation are considered in particular. Section 2 discusses the case of mass transport influenced electron-transfer kinetics in the absence of any chemical reactions; Section 3 discusses the theoretical understanding of the

interplay between mass transport and the chemical reactions; Section 4 shows the electrochemical response influenced by the mass transport in some illustrative electrocatalytic systems. The details of simulation method are not reviewed here but are covered in two books[7-8] as well as, in the case of COMSOL modelling, a short review.[9]

2 The Influence of Mass Transport on Heterogeneous Electron Transfer

2.1 Electron-Transfer Kinetics under the Influence of Diffusion

At a nanoelectrode where the diffusion is significantly enhanced in comparison with macrosized electrodes, quicker heterogeneous electron transfer kinetics can be measured and quantified. The different current-voltage responses from two commonly-used electron-transfer kinetic models for a simple one-electron-transfer reaction Red + e^- = Ox are compared here. In the classical Butler-Volmer(BV) model, the reductive and oxidative electron-transfer rate constants $k_{red/ox}$ increase exponentially with the overpotential η (η is the difference between the applied potential E and the formal potential E_f, $E - E_f$):

$$k_{red} = k_0 \exp\left(-\frac{\alpha F \eta}{RT}\right); k_{ox} = k_0 \exp\left(\frac{(1-\alpha) F \eta}{RT}\right) \quad (1)$$

where k_0 is the standard electrochemical rate constant and α is the transfer coefficient. The current on nanoelectrodes is always limited by diffusion at high overpotential and reaches a steady-state value I_{ss}. The diffusion-controlled I_{ss} is

independent of k_0 and α. The influence of the electron-transfer kinetics is reflected in the position of the half-wave (where $I = I_{ss}/2$) potential and the voltammetric wave shape. k_0 and α can be derived via fitting the experimental potential-dependent response from simulation.[10-11]

In contrast, in the Marcus-Hush-Chidsey(MHC) model, the reaction rate cannot infinitely increase with overpotential due to the limitation of the solvent and/or ligand reorganization. Taking the symmetric MHC model as an example, the reductive or oxidative electron-transfer rate constant (k_{red}/k_{ox}) can be expressed as:[12]

$$\frac{k^*_{red/ox}}{k^*_0} = \frac{\int_{-\infty}^{+\infty} \frac{1}{1+\exp\left(\mp\varepsilon^*\right)} \exp\left(-\Delta G^*_{red/ox}\right) d\varepsilon^*}{\int_{-\infty}^{+\infty} \frac{1}{1+\exp\left(\mp\varepsilon^*\right)} \exp\left(-\Delta G^*_{red/ox}\left(\eta^* = 0\right)\right) d\varepsilon^*} \tag{2}$$

$$\Delta G^*_{red/ox} = \frac{\lambda^*}{4}\left(1 \pm \frac{\eta^* + \varepsilon^*}{2}\right)^2 \tag{3}$$

k_0 is the heterogeneous electron-transfer rate constant and λ is the reorganization energy. The other symbols are defined in Table 1. The dimensionless form (marked by *) is used to avoid selecting any experimental conditions in the discussion. The dimensionless parameter k_0^* involves the influence of the electrode radius r and the reactant diffusion coefficient D, as defined in Table 1.

The current-voltage response of the symmetric MHC model for a one-electron-transfer reaction on a nanosphere electrode is illustrated in Figure 1. The results of BV model are shown by dashed lines for comparison. The current is calculated by solving the diffusion equation (Fick's second law) under the boundary

condition of Eqn.(1) (BV) or Eqn.(2) (symmetric MHC). The diffusion-controlled I_{ss}^{*} = 4π. When decreasing k_0^{*}, the BV model leads to a potential shift towards higher overpotential and I_{ss}^{*} equals the diffusion-controlled value; while in the MHC model, the overpotential increases and I_{ss}^{*} becomes much smaller than the diffusion-controlled value. In the MHC model, λ^{*} reflects the hindrance of the electron transfer and decreasing λ^{*} also leads to smaller currents. For an irreversible electron-transfer, the kinetically-limited I_{ss}^{*}, which is smaller than 4π, can be observed for small k_0^{*} or λ^{*}, as the reductive and oxidative rate constants of high overpotentials are limited by the solvent or ligand reorganization.[12] As shown in Figure 1b and 1d, the rate constants of the BV model varies exponentially as a function of the overpotential and leads to a linear Tafel plot; while those of the MHC model stops increasing at high overpotentials, generating a curved Tafel plot. The influence of the electrode size on the current response is involved in k_0^{*}. For a smaller nanoelectrode, it becomes more possible to observe a kinetically-limited I_{ss}. The solvent reorganization energy and the electron transfer rate constant can be detected in principle via simulation of a kinetically-limited I_{ss} and the current-voltage response measured from the nanoelectrode.[13]

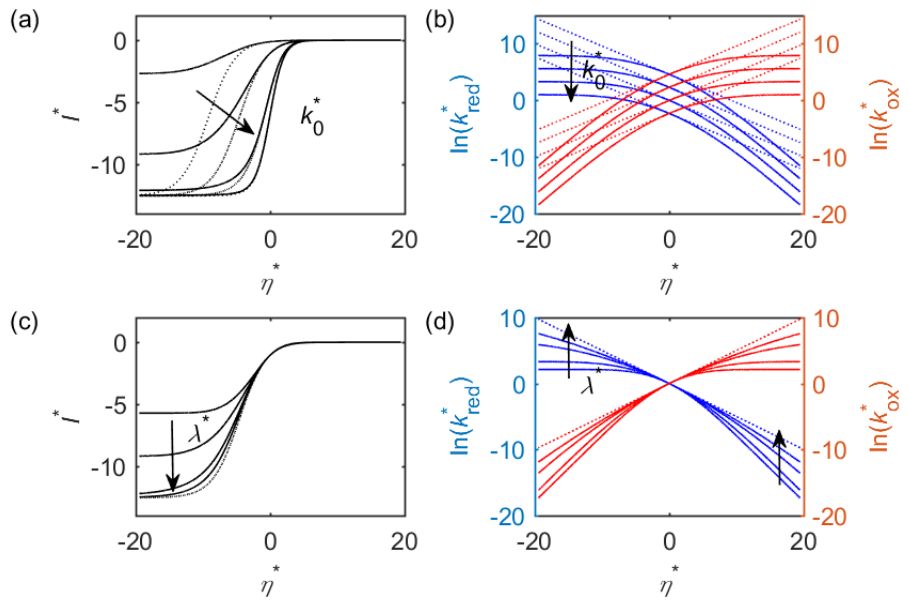

Figure 1 (a) Current-voltage responses of the MHC model with a variable k_0^* (k_0^* = 10^{-1}, 1, 10^1, 10^2 from top to bottom); (b) Potential dependence of the reductive (blue) and oxidative (red) rate constants with a variable k_0^*; (c) and (d) are the corresponding results of when λ^* increases from 4 to 80 (λ^* = 4, 8, 20, 40). λ^* used in (a) and (b) is 8; k_0^* used in (c) and (d) is 1. The dashed lines are the current responses and the kinetic rate constants based on the BV model.

In symmetric MHC model shown in Figure 1, the activation energy $\Delta G_{red/ox}^*$ has the same potential dependence for the reductive and oxidative processes. The activation energy in the asymmetric MHC model shows different potential dependences on the reductive and oxidative directions:[14]

$$\Delta G_{red/ox}^* = \frac{\lambda^*}{4}\left(1 \pm \frac{\eta^* + \varepsilon^*}{2}\right)^2 + \beta^*\left(\frac{\eta^* + \varepsilon^*}{4\lambda^*}\right)\left\{1 - \left(\frac{\eta^* + \varepsilon^*}{\lambda^*}\right)^2\right\} + \frac{\beta^{*2}}{16\lambda^*} \quad (4)$$

where the dimensionless parameter β^* represents the divergence of the curvatures of the symmetric Gibbs energy curves. For free diffusing redox species, BV and asymmetric MHC models both perform well fitting to the experimental data.[15] The asymmetric MHC theory provides physical insight for the phenomenological BV model. However, for the surface bound electron-transfer systems, the asymmetric MHC model invariably fits the voltammograms much better than the BV model,[16] which needs to be considered when interpreting such experimental data.

2.2 Structure and Activity Studies of Single Nanoentities

In diffusion-controlled situations, the geometry and the size of the electrode can be readily characterised by the steady-state current I_{ss}. For a diffusional reversible one-electron-transfer condition, the steady-state current can be expressed as:

$$I_{ss} = \frac{FSDc_{bulk}}{\delta_{geo} r} \tag{5}$$

where D is the diffusion coefficient, S is the electrode area and δ_{geo} is the geometry factor. The electrode geometry influence on the diffusion-controlled current response can be quantified via δ_{geo} (some literature uses "effective radius" instead).[17-19] The values of δ_{geo} for some commonly-used geometries are shown in Figure 2. r is the radius of the spherical, hemispherical and disc electrode or the side length of a square electrode. Note that Eqn.(5) only works for electrodes with known, simple geometries as shown in Figure 2 and that r is usually treated

as the "effective radius" in real applications. On the other hand, for a given geometry, the size of a nanoelectrode can be measured from experiment by using fast redox species such as aqueous $Ru(NH_3)_6^{2+/3+}$ in a fully-supported electrolyte solution.[20-21]

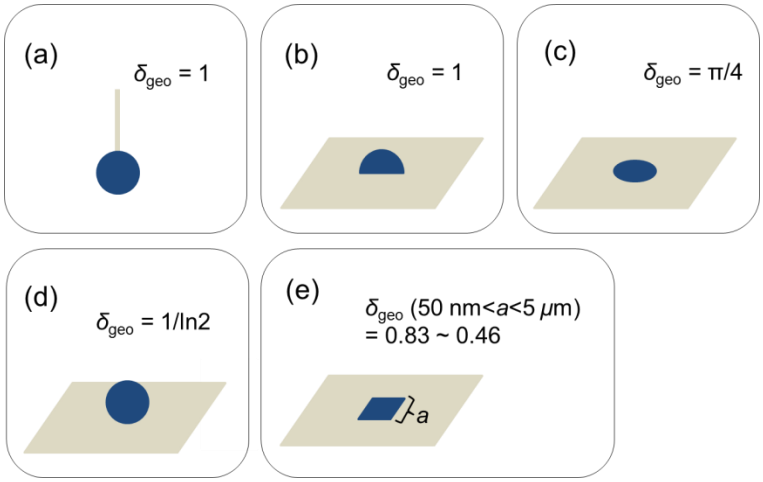

Figure 2 Five commonly-used nanoelectrode geometries and corresponding geometry factors δ_{geo}.[18-19, 22] (a) Isolated sphere; (b) Hemisphere attached on a supporting substrate; (c) Planar disk; (d) Sphere attached on a supporting substrate; (e) Square with an area of a^2. Blue: Electroactive materials; Grey: Inert substrate. The electron transfer only takes place on electroactive materials.

Via fitting a simulation model to the experiment data, the electrocatalytic kinetic parameters, such as the electron-transfer rate constant and the transfer coefficient (or the reorganization energy), can be measured on single nanoelectrodes, even for fast heterogeneous electron transfer reactions such as $Ru(NH_3)_6^{2+/3+}$, $FcCOOH^{0/+}$, $Fe(CN)_6^{4-/3-}$.[23-24] With these fast redox reactions, the

electrocatalytic activity of nanoelectrodes can be estimated and compared among different materials.[25-27] Linking the electrocatalytic ability with the size or the geometry of the nanoelectrode is useful for better understanding structure–function relationship of nano-electrocatalysts. Zhang et al measured the electron-transfer rate constants of $Ru(NH_3)_6^{2+/3+}$ and $Fe(CN)_6^{4-/3-}$ at graphene flakes with various sizes to explore the size dependence electron-transfer kinetics.[26] Similar measurements were implemented on Au and Pt nanoparticles of various sizes,[28] linking the crystalline structure with nanoparticle electrocatalytic ability.

2.3 Interplay between Diffusion and Migration

The above two sections discuss diffusional mass transport in fully-supported electrolyte solution. However, in solutions with low electrolyte concentration and for small electrodes, the influence of the electrical field at the electrode-electrolyte interface also needs to be considered. For a nanoscale electrode, the thickness of the diffusion layer can be comparable to the thickness of the electrical double layer which is established in response to electrical charging of the electrode, and the migration of charged species driven by the electrical field cannot be neglected.[29] The Debye length κ^{-1} is used to characterise the thickness of the electrical double layer at equilibrium (when no net charge through the electrode interface). κ^{-1} is independent of r_{el} but proportional to the inverse square root of the ionic concentration $c_{elec}^{-1/2}$:

$$\kappa^{-1} = \sqrt{\frac{RT\varepsilon_s\varepsilon_0}{2F^2 c_{\text{elec}}}} \tag{6}$$

ε_s and ε_0 are the local dielectric constant and the permittivity of a vacuum.

Dickinson et al comprehensively investigated the influence of the diffuse layer on the passage of Faradaic current for steady-state voltammetry, in aspects of both the mass transport via electrostatically attracting or excluding the reactant (Levich exclusion effect) and the electron-transfer rate via altering the effective activation energy of charge transfer (Frumkin correction).[30] The later was originally analysed by Frumkin in case of electron transfer occurring exclusively at a fixed 'plane of electron transfer (PET)', a given distance from the electrode. With the involvement of the migration, the electrode flux of a redox reaction $\mathrm{A}^{z_\mathrm{A}} + \left(z_\mathrm{A} - z_\mathrm{B}\right)e^- \underset{k_{\text{ox}}}{\overset{k_{\text{red}}}{\rightleftharpoons}} \mathrm{B}^{z_\mathrm{B}}$ can be written as:

$$\frac{j}{z_\mathrm{A} - z_\mathrm{B}} = k_{\text{red}} c_\mathrm{A}^{\text{PET}} - k_{\text{ox}} c_\mathrm{B}^{\text{PET}} \tag{7}$$

j is the current flux. $c_\mathrm{A}^{\text{PET}}$ and $c_\mathrm{B}^{\text{PET}}$ are the concentrations of A and B at a so-called plane of electron transfer, where the electron transfer occurs. The concentration at PET can be solved computationally by the Nernst-Planck equations.

$$j = D\nabla c + \frac{zcDF}{RT}\nabla\phi \tag{8}$$

$$\frac{\partial c}{\partial t} = \nabla j = D\nabla^2 c + \nabla\left(\frac{zcDF}{RT}\nabla\phi\right) \tag{9}$$

where ϕ is the local potential in solution. The potential distribution in solution is determined by the local charge, described by the Poisson equation:

$$\nabla^2\phi = \frac{1}{\varepsilon_s\varepsilon_0}\sum zC \tag{10}$$

By solving Eqn.(9) and Eqn.(10) (the Nernst-Planck-Poisson equation) under the boundary condition of Eqn.(7), the concentration and potential distributions in the solution phase can be calculated. The solution-phase potential is a function of the applied potential E and the potential of zero charge E_{pzc}. E-E_{pzc} reflects the excess charge of the electrode, which affects the distribution of the potential and concentration of ions in the double layer.

The migration of the charged reactant is observed towards (where $z_A(z_A\text{-}z_B)>0$) or repelled (where $z_A(z_A\text{-}z_B)<0$) from PET due to the excess charge on the electrode surface, leading to an increase or decrease of the current compared to the result in the fully-supported solution; while the neutral reactant (where $z_A = 0$) is independent of the migration influence. Varying E_{pzc} affects the current response via intensifying or decreasing the electrostatic interaction between the electrode and the redox ion. In contrast to the typical steady-state current plateaux on nanoelectrodes in fully supported electrolyte solution, peak-shaped current responses where the current decreases at high overpotentials are simulated for the oxidation of a positively charged reactant and the reduction of a negatively charged reactant, showing the competition between the migration exclusion and the diffusion towards the electrode.

The influence of the electrical double layer on the electrochemical reaction is also reflected on the apparent electron-transfer kinetics due to the potential drop within the double layer, as considered in the Frumkin correction. The potential "driving" the electron transfer is the potential drop between the electrode surface and PET, E - ϕ_{PET}. For reactions in insufficiently-supported electrolyte solution, when calculating the rate constants $k_{red/ox}$ in the boundary condition Eqn.(7), the potential drop applied in either BV or MHC theory is not E but E - ϕ_{PET}. It is found that the current decreases from the diffusion-controlled I_{ss} as the consequence of the kinetically-limited electron transfer rates at PET. When the electron-transfer rate is finite, the current response to the migration is also a function of electrode radius and the voltammetric response deviates more from the diffusion-controlled result on the nanoelectrode with a smaller size.[31]

In reality electron transfer through tunnelling to or from the electrode rather than occurring at a single plane (PET). The tunnelling probability usually is assumed on the basis of experiment to have a distance dependence of exp(-$\beta' x$) where β' is the tunnelling decay constant and x is the distance from the electrode.[32] For aqueous solution, β' is approximately 1.6 Å. The electron tunnelling near the electrode surface spatially extends the effective electron-transfer region and this increases the current at high overpotentials.[30, 33] Overall the effect of including the realistic description of electron transfer eventually is to substantially mitigate the Frumkin effect as originally modelled by Frumkin.

The experimental interpretation of the EDL is rather difficult due to the multiple factors affecting the current response and the uncertainties in the many parameters which quantify the EDL parameters as mentioned above. Recent

study by Bae et al reported the influence of EDL on the voltammograms for highly charged redox species $Fe(CN)_6^{4-/3-}$ in 1 M KCl solution, showing that the measurement of k_0 in such conditions needs to be corrected for the EDL effect.[34]

2.4 Competition among Nano-Diffusion, Linear Diffusion and Thin-Layer Diffusion regimes

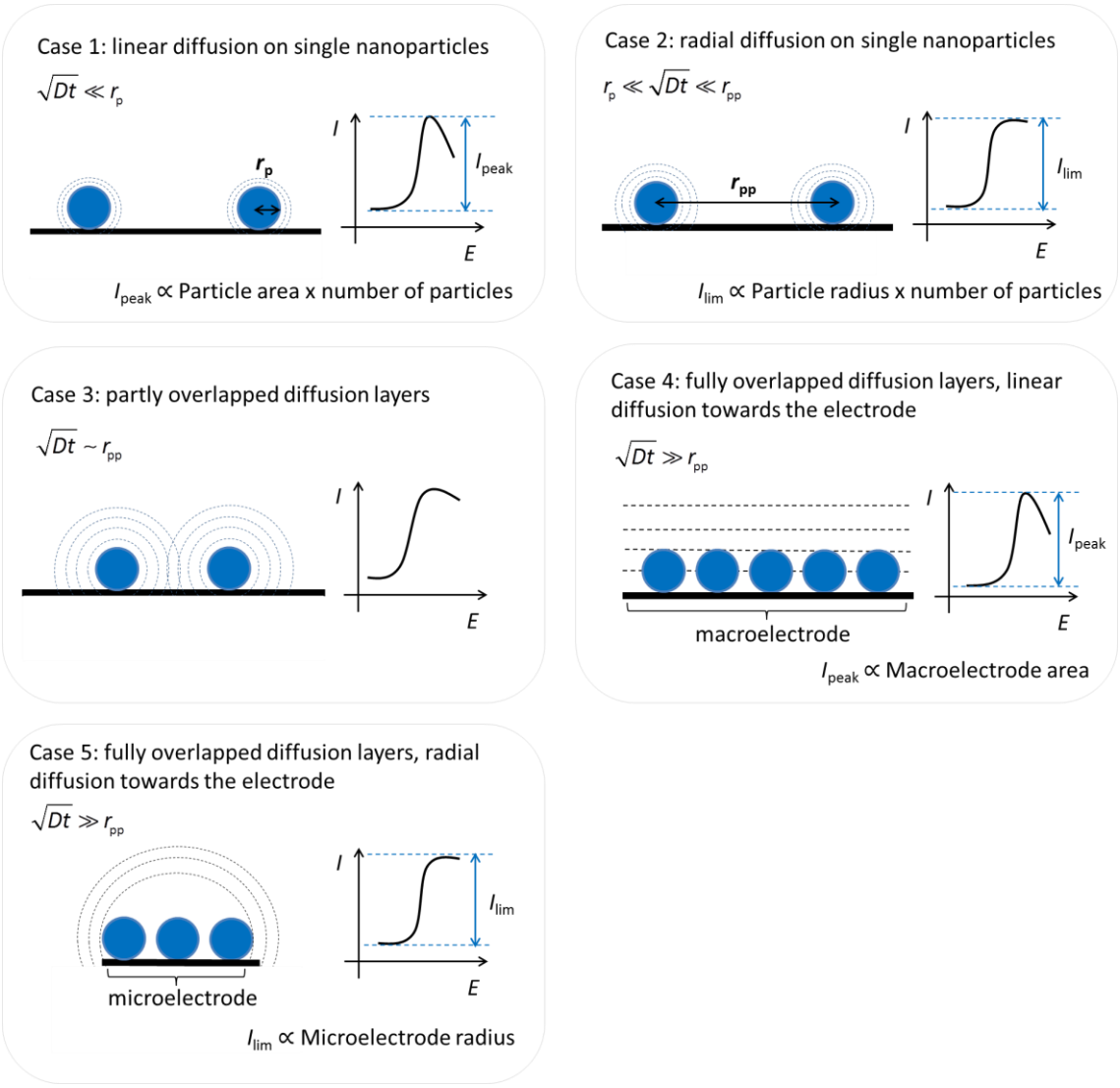

Figure 3 The five diffusion regimes for nanoparticles attached on the substrate electrode. The spheres are nanoparticles and the dashed line indicates the diffusion layer.

Even considering only solely diffusional mass transport, various competing diffusion regimes can appear on an electrode with a non-simple geometry. Figure 3 illustrates five cases for spherical nanoparticles, in the form of an array, attached to an inert substrate electrode in respect of various diffusion regimes.[35-36] It is assumed that electron transfer only takes place at the nanoparticle surface; the conducting electrode acts only as a physical support and to electrically contact the particle. The qualitative current-potential responses of each case are also illustrated in Figure 3.

Case 1 corresponds to the linear diffusion towards single nanoparticles and is seen at short timescales or under fast scan rates, where 'short' means $\sqrt{Dt} \ll r_p$ (r_p is the radius of the nanoparticle). Case 2 reflects the radial diffusion towards single nanoparticles, which can be observed when $r_p \ll \sqrt{Dt} \ll r_{pp}$ (r_{pp} is the interparticle distance). The current-voltage response of the entire array is similar to that of the isolated particles but scaled by their numbers. The current from each single nanoparticle in Case 2 is the same as the shielded spherical nanoelectrode in Figure 2d. Case 3 shows the case of overlapped diffusion layers for nanoparticles close to each other, as a mixture of the radial diffusion towards single nanoparticles and the linear diffusion towards the entire electrode. In this case, $\sqrt{Dt}$ is the same order of magnitude of r_{pp}. Case 4 is the case of linear

diffusion towards the entire electrode as a consequence of fully overlapped diffusion layers of adjacent nanoparticles on a *macroelectrode*, where $\sqrt{Dt} \gg r_{pp}$. The current-voltage response is almost identical to that of a macroelectrode of the same geometric radius as the modified electrode. Finally, Case 5 describes the situation of nanoparticles assembled on a *microelectrode*. On a microelectrode, when the diffusion layers of each nanoparticles overlap under high nanoparticle coverages and moderate scan rates ($\sqrt{Dt} \gg r_{pp}$), the diffusion layer of the whole array is hemispherical rather than linear, where the radial diffusion is reflected by the sigmoidal current-voltage curve measured from the nanoparticle arrays modified on microelectrodes.[37]

Recent work by Costentin et al modelled the competition between a linear diffusion towards the substrate electrode and nanodiffusion (convergent diffusion) towards each single electroactive nanoparticle attached to an electrode.[38] By varying the scan rate and the nanoparticle density on the electrode, the overall behaviour of the electrode system is manipulated between purely radial diffusion (case 2 in Figure 2) and linear diffusion (case 4). In the mixed radial and linear diffusions (case 3), the catalytic effect is determined by the competition between the two diffusion regimes. For irreversible electron-transfer reactions, the apparent electron-transfer rate constant is a function of the ratio of the total electroactive surface area to the geometric area of the substrate electrode itself Ψ. An apparent positive catalytic effect reflected by the peak potential shifting closer to the formal potential is observed at $\Psi > 1$; while the current-voltage response of $\Psi < 1$ performs a negative catalytic effect, where the overpotential required for the current peak increases.[39]

If the electroactive nanomaterial composes a porous multilayer structure on an inert substrate electrode, the diffusion through the porous layer leads to different current responses from the semi-infinite diffusion towards a planar electrode. Different behaviour is seen for porous layers which are electrically conductive, carrying out electrolysis and insulating layers. On conductive porous electrodes, when the diffusion inside the porous layer is not efficient, the porous structure becomes the analogue of "thin layer" transport. Typical examples were reported for carbon nanotubes modified electrodes.[40-42] Symmetric forward and backward voltammetric peaks are the typical feature of ideal thin-layer diffusion. Compared to the semi-infinite diffusion, a smaller peak-to-peak separation and a higher peak current can be observed from the voltammograms on porous electrodes.[43] Importantly, the voltammogram of the thin-layer diffusion effect can be easily misdiagnosed as the catalytic influence with respect to the reduced peak-to-peak separation and the increased peak current.[41, 43]

More challenging situations can be found in electrodes covered by the insulating porous nanomaterials. In contrast to the electroactive porous layer as discussed above, the redox reaction only takes place on the supporting electrode surface, where the attached nanoparticles work as blockers rather than catalysts. The measured current response is smaller than that on the bare substrate electrode. However, it is interesting that under certain conditions, a false impression of 'improved electrocatalysis' in respect with the decreased peak-to-peak separation can be observed on electrodes covered by insulating porous layers.[44-46] If the reactant can be adsorbed on the insulating porous layer surface, the amplification of the current can be several times larger than the semi-infinite

diffusion result,[47] depending on the scan rate, the adsorption area and the adsorption rate, but it is unlikely to realise an order of magnitude enhancement unless multilayer adsorption is present.[48] Again note that the insulating porous structure can mislead the experimenter and give the impression of the electrocatalytic ability. Therefore, careful interpretations of such voltammograms are required ideally comparing simulation and experiment if physical or chemical insight is sought.

Although in this section only diffusional mass transport is discussed, other mass transport effects may also need to be considered when using nanoparticle modified electrodes. For instance, when the nanoparticle and the supporting substrate are two different materials, the particle proximity effect due to the different surface charging properties can be observed, especially for small (i.e. a few nm diameter) nanoparticles which are close to each other and form overlapped EDLs.[49] In absence of the diffusion influence, it is found that the electrocatalysis of the nanoparticles depends on the nanoparticle size, coverage and the electronic properties of both the nanoparticle and the supporting material. The electrocatalytic activity of the nanoparticle modified electrode can be significantly enhanced by increasing the surface coverage.[50] Future study of the combination and interplay of electrostatic and diffusional effects on the electrocatalysis of nanoparticle modified electrodes will be very helpful in understanding the interface kinetics, although simulating such system is really challenging and the selection of correct boundary conditions to describe the electrode-electrolyte interface needs to be carefully considered.

3 The Interplay between Diffusion and Chemical Reaction in Electrocatalytic Reactions

For more complicated electrocatalytic reactions, electron transfer follows or triggers a chemical reaction, where the current response is also affected by the kinetics and thermodynamics of the chemical reaction.[51-52] The molecular catalysis reaction (also called the EC' reaction) is a typical example,[53] where the redox species exchange electrons with the electrode and act as the catalyst in the reaction of other solution-phase species:

$$A + e^- \rightleftharpoons B \tag{11}$$

$$B + R \xrightarrow{k_c} A + P \tag{12}$$

where A/B are the redox couple, R is the solution-phase reactant and P is its product. k_c is the rate constant of the catalytic step (mM^{-1} s^{-1}/mol m^{-3} s^{-1}). The redox species can be either in the solution phase or attached to the electrode surface.

When A and B are solution-phase redox species, under moderate scan rates, the cyclic voltammogram is a sigmoidal curve and the steady-state current at the nanoelectrode can be approximated as: [54]

$$\frac{I_{ss}^*}{I_{ss,1e}^*} = 1 + \frac{\sqrt{k_c^*}}{\frac{1}{\delta_{geo}} + \frac{\sqrt{k_c^*}}{\gamma_{AR}}} \tag{13}$$

$I_{ss,1e}^*$ is the corresponding diffusion-controlled steady-state current for one-electron-transfer reactions (Eqn.(5)). The dimensionless parameter k_c^* reflects the size effects on the catalytic reaction rate while γ_{AR} is related to the excess of the reactant relative to the redox catalyst.

$$k_c^* = \frac{k_c c_R r^2}{D_A} \tag{14}$$

$$\gamma_{AR} = \frac{c_R D_R}{c_A D_A} \tag{15}$$

where c_A and c_R are the bulk concentrations of the redox catalyst A and the reactant R, D_A and D_R are the diffusion coefficients of A and R. When the redox couple A/B in the EC' reaction is immobilized at the electrode, the current at high overpotentials can be expressed as: [55]

$$\frac{I_{ss}^*}{I_{ss,1e}^*} = \frac{k_c'^*}{\frac{1}{\delta_{geo}} + k_c'^*} \tag{16}$$

$$k_c'^* = \frac{k_c' \Gamma_{max} r}{D_A} \tag{17}$$

where Γ_{max} is the maximum surface coverage of the adsorbed redox species on the electrode and k_c' is the catalytic rate constant ($mM^{-1}\ s^{-1}$) of the immobilized A/B. Eqn. (13) and Eqn.(16) are examples of current responses at high overpotentials for the diffusion-coupled EC' reactions on nanoelectrodes. As the electrode size r is involved in k_c^* and $k_c'^*$, varying r can change the steady-state current and lead to different results on the apparent number of electrons transferred in an EC' reaction.

The ECE reaction is another important example:

$$A + e^- \rightleftarrows B\ ,\ E_{f,\,A/B} \tag{18}$$

$$B \underset{k_b}{\overset{k_f}{\rightleftarrows}} C \tag{19}$$

$$C + e^- \rightleftarrows D\ ,\ E_{f,\,C/D} \tag{20}$$

where E_f is the formal potential, k_f and k_b are the forward and backward rate constants of the chemical step. The intermediates B and C can be either solution-phase species or attached on the electrode surface. Assumed that the two redox processes are fast, two separated voltammetric waves may be observed on a nanoelectrode, depending on the diffusion (D, r), the kinetics (k_f, k_b) and the thermodynamics (k_f/k_b) of the chemical reaction and the formal potential difference ($E_{f,\,C/D}$ - $E_{f,\,A/B}$) between the two electron-transfer steps.[56] The limiting current at high overpotentials for the ECE process is $1 < I_{ss}^*/I_{ss,1e}^* < 2$. Similar to the EC' system, the apparent number of electrons transferred in the ECE reaction on nano-particles/electrodes can be manipulated by altering the electrode size r.

4 Nano-Electrocatalysis

4.1 Joint Experimental and Computational Study in the Search for Authentic Nano-Electrocatalytic Effects

By comparing the electrocatalytic kinetics measured from both the macro- and nanosized electrodes made of the same materials, the authentication of any electrocatalytic nanoeffect can be determined. The combination of experimental and computational studies enables the quantification of the kinetic parameters as introduced in Section 2. Mass transport effects must be decoupled in order to identify authentic catalysis since the electrode size and the electrode modification in making nanoparticle arrays inevitably alter the transport conditions away from semi-infinite and influence the kinetic analysis.[36, 57] A joint experiment and simulation study was implemented on gold nanoparticle arrays and gold macroelectrodes for the electrooxidation of nitrite and L-ascorbate, the procedure of which is shown in Figure 4.[58] By comparing the kinetics measured from the Au macroelectrode and Au nanoparticles via both experiment and simulation, it was found that there was no nanoeffect for the nitrite oxidation but an enhanced electrocatalytic current was observed on the electrooxidation of the L-ascorbic acid. The possible explanation is that L-ascorbic acid oxidation involves adsorption and therefore the current response is sensitive to the electrocatalyst structure. The quantitative comparison of the kinetics at macro- and nanosized electrodes is of great interest to elucidate the fundamental aspects of naoneffects on the electrocatalysis.

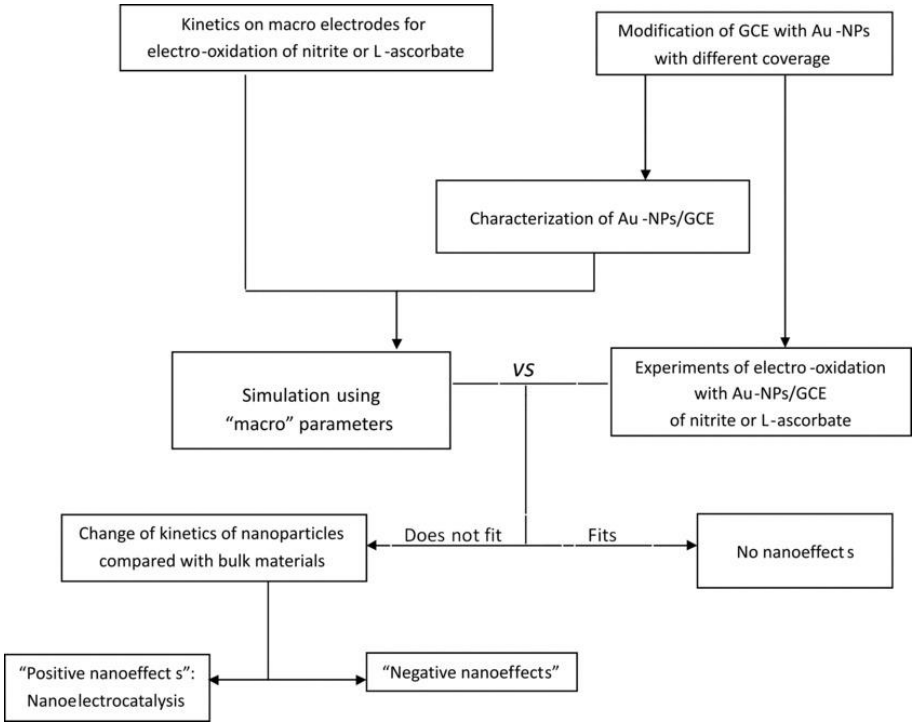

Figure 4 Approach followed in this work for the detection of nanoelectrocatalysis of the electrooxidation of nitrite and L-ascorbate by gold nanoparticles combining electrochemical measurements with computational simulations. Reproduced with permission from ref 56, 2013, Wiley-VCH.

Kinetic studies of some electrocatalytic systems are discussed in this section. The interfacial kinetics, the electrocatalytic nanoeffect, and the selectivity variation on nano-electrocatalyst are particularly considered.

4.2 Hydrogen Evolution and Oxidation Reactions

The hydrogen evolution/oxidation reaction (HER/HOR) $2H^+ + 2e^- \rightleftarrows H_2$ contains three possible elementary steps:

$$H^+(sol) + e^- \rightleftarrows H(ads) \text{ (Volmer)} \quad (21)$$

$$H(ads) + H^+ + e^- \rightleftarrows H_2(sol) \text{ (Heyrovsky)} \quad (22)$$

$$H(ads) + H(ads) \rightleftarrows H_2(sol) \text{ (Tafel)} \quad (23)$$

where H^+(sol), H_2(sol) and H(ads) are the proton, dissolved di-hydrogen and adsorbed hydrogen.

By comparing the steady-state current values between the experimental measurement from single platinum nanoparticles (PtNPs) and the simulated results, the mechanism of HOR on PtNPs has been shown to follow the Tafel-Volmer reaction.[59-60] At high overpotentials, the steady-state current is much smaller than the diffusion-controlled value, indicating that the adsorption of hydrogen on Pt, rather than the mass transport of hydrogen towards the electrode, is the rate-determining step of HOR on PtNPs. The adsorption rate constant was also measured from the steady-state current.

Measurement of current responses on single nanoparticles provides information of the interface dynamics and the nanoeffect for HER. Zhou et at applied the nanoimpact technique to detect the nanoeffect of HER on single Ni@NiO nanoparticles.[61] The potential-dependent catalytic current measured at single Ni@NiO nanoparticles shows similar kinetics to that seen on a NiO microelectrode surface, indicating no size effect or nanoeffect for HER on the Ni@NiO nanoparticles. However, a negative effect was observed for HER on 2 nm Au nanoparticles, where k_0 decreases one order of magnitude comparing to the

gold macroelectrode.[62] Recent work by Xiang et al studied the transient response of HER on single PtNPs under He and H_2 atmospheres.[63] Compared to the He atmosphere, a slower HER electrocatalysis under H_2 atmosphere was observed, showing the passivation effect caused by the hydrogen adsorption on PtNPs.

4.3 Oxygen Reduction Reaction

The two possible generic reaction paths of the oxygen reduction reaction (ORR) according to the study of Wroblowa as shown in Scheme 1.[64] The direct pathway is the direction reduction to water with four electrons transferred; the indirect reduction first generates the intermediate H_2O_2 with two electrons transferred and then H_2O_2 is further reduced to water. Chen and Kucernak simulated the indirect ORR on carbon supported single PtNPs and reported that all the reactant O_2 was reduced to water under low mass transport conditions while only a portion of the reactant became water and the rest was reduced to H_2O_2 under high mass transport.[65] The enhancement of mass transport for the ORR actually decreases the effective number of electrons transferred on a nanoelectrode, as the result of the variation of mass transport for the diffusional intermediate H_2O_2. The conclusions made in respect of the single nanoparticles also relates to the ORR on nanoparticle modified electrodes, where more H_2O_2 is formed with smaller nanoparticles and larger interparticle distances (both increases the mass transport efficiency) of the nanoparticle array.[66-67]

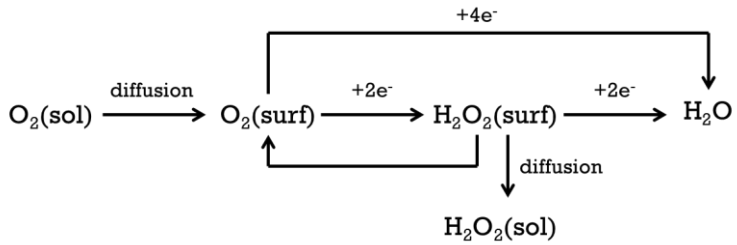

Scheme 1 Wroblowa scheme[64] of the direct and indirect reaction paths for oxygen reduction reaction.

Nanoeffects on the ORR kinetics for a series of gold nanoparticles (AuNP) of 2~40 nm radii were investigated by Compton et al via comparing the kinetic parameters measured from AuNP modified electrodes and a gold macroelectrode.[62, 68-69] The mechanism of ORR was inferred to be the two-electron-two-proton transfer mechanism and the product to be H_2O_2:[68]

$$O_2 + e^- \rightleftharpoons O_2^{-\bullet} \quad (24)$$

$$O_2^{-\bullet} + H^+ \rightleftharpoons HO_2^{\bullet} \quad (25)$$

$$HO_2^{\bullet} + e^- \rightleftharpoons HO_2^- \quad (26)$$

$$HO_2^- + H^+ \rightleftharpoons H_2O_2 \quad (27)$$

The first step was regarded as the rate-determining step. The electron-transfer rate constant of the rate-determining step and the transfer coefficient measured from AuNPs of 5~40 nm radii are almost identical with the results on the Au macroelectrode, showing there is no significant nanoeffect on the electrocatalytic

kinetics for ORR on Au.[68-69] However, a negative effect was found for 2 nm AuNPs, where the electron-transfer rate constant of the rate-determining step is two orders of magnitude smaller than measured from the Au macroelectrode.[62]

4.4 Carbon Dioxide Reduction Reaction

Developing effective and highly-selective electrocatalysts for CO_2 reduction is of significant interest for energy and environment. CO_2 can be reduced to either CO or HCOO(H), depending on the catalyst, the reaction conditions and the overpotential.[70] However, the reduction of CO_2 involves the electro-hydrogenation by the adsorbed hydrogen on the electrode surface, which also leads to the evolution of hydrogen and the generation of hydrocarbons such as CH_4 and C_2H_4.[71] Therefore, the selectivity of certain CO_2 reduction product becomes an important feature for any catalyst. The selectivity can be manipulated by not only varying the catalytic ability but also adjusting the mass transport conditions on the electrode.[72-73] The Faraday efficiency for producing CO or $HCOO^-$ is closely related to the diffusion conditions of the electrode interface, where more CO or $HCOO^-$ is usually found on nanoparticles with smaller sizes or larger interparticle distances on nanoparticle modified electrodes.

The microkinetics of CO_2 electroreduction on nanoparticles was investigated for the better understanding the kinetics factors affecting the reaction selectivity and the rate-determining step. Recent studies have been reported for CO_2 reduction on sharp-tip Au nanostructures, where CO_2 is reduced to CO.[74-75] Liu et al proved that applying a high-curvature nanostructure and adding the cationic

ion K^+ in the solution could dramatically improve the current density.[74] Simulation shows that the sharp-tip structure causes large electrical field on the tip, where the enhanced electrostatic field was thought to increase the mass transport and surface adsorption of K^+. DFT calculations reveal that K^+ is able to stabilize the reaction intermediate and thus decreases the reaction barrier needed for the formation of the intermediate. A diffusion-reaction model applied by Jiang et al revealed the electrocatalytic behaviour were improved because of both the lowered the reaction barrier and the increased the mass transport of CO_2.[75] It was also reported that due to the fast reaction rate on the nanostructure surface, the insufficiency of CO_2 mass transport rather than the reaction barrier was the rate-determining factor. The simulation of the mass transport influenced reaction kinetics provides a direct approach to explore factors influencing the reaction selectivity and the rate-determining step in the overall electrocatalytic system.

5 State-of-the-Arts and Limitations

The preceding sections illustrate that the pursuit of a synergistic approach between theory and experiment is within modern computational scope and that such an approach allows a definitive evaluation of the physical and chemical models which relate to electrocatalysis. The recent and current literature is replete with examples of qualitative, semi-qualitative and empirical studies. These have their roles in advancing some technology but the deeper interplay of theory and experiment is essential in order to probe fundamentals and to drive informed advances. Refs 7-9 show that the necessary computational techniques exist provided the user is willing to invest the effect in learning simulation, although some analysis, especially in limiting cases, can be achieved by analytical theory[76] whilst commercial simulation softwares provide a semi-quantitative approach valuably used in exploratory simulations.[77] For example, analytical theory has been impressively displayed by Molina and colleagues to understand pulse voltammetry and its applications[78]; whilst COMSOL has been used successfully to explore the essential role of temperature control particularly in SECM experiments, where imperfect thermostatting is known to contribute to some misleading results owing to density driven convection currents.[79] Similarly, the finite difference software such as DIGISIM, pioneered by M. Rudolph,[80] is extremely useful for the simulation of some voltammetric problems relating to isolated single electrodes.[81-82] However the temptation to include a surfeit of reactions is sometimes found to be irresistible whilst the inclusion of adsorption effects and of usually requires self-written software, although the KISSA program offers an off-the-shelf approach to the analysis of adsorption process.[83] Enhancing

studies of electrocatalysis at the single-nanoparticle or even molecular levels will require stochastic simulations, where higher-performing parallel computation (such as the application of Graphics Processing Units),[84] the consideration of possible effects of potentiostat hardware (such as the filter),[85] and the case-by-case data processing procedure designed according to the real experimental environment[86] are often emphasized in self-written programs.

6 Concluding Perspectives

Recent studies of the electrocatalysis on nanoparticles and nanoelectrodes under the influence of the mass transport were briefly discussed. One difficulty of understanding the electrocatalytic ability on nanomaterials is to need to clarify and separate the mass transport influence and any nanoeffect related to the electronics of the catalyst, especially for complex electrode geometries. The combination of experiment and simulation enables us to quantify the kinetics of electrocatalysis and thus indicates information such as the interfacial dynamics of an electrochemical reaction or the structure-dependent activity of the electrocatalyst. A close synergy between simulation and experiment is desirable for the rigorous development of new electrocatalysts and for understanding key electrode processes.

Table 1 Dimensional and dimensionless variables.

Symbol	**Interpretation**
I	Current
I_{ss}	Steady-state current
$I_{ss,1e}$	Diffusional steady-state current of one electron transfer
$k_{red/ox}$	Reductive/Oxidative electron-transfer rate constant
η	Overpotential
E	Electrode potential
E_f	Formal potential
k_0	Standard heterogeneous electrochemical rate constant
α	Transfer Coefficient
λ	Reorganization energy
ε	Metallic energy level
F	Faraday constant
R	Gas constant
T	Room temperature
D	Diffusion coefficient
r	Electrode radius of a spherical/circular area or side length of a square area
c_{bulk}	Bulk concentration
c	Concentration
δ_{geo}	Geometric coefficient
κ^{-1}	Debye length
j	Current flux
z	Charge
ϕ	Local potential in solution
ε_s	Local static dielectric constant
ε_r	Permittivity of a vacuum
x	Distance from the electrode
k_c	Second-order rate constant of the EC' reaction
Γ_{max}	Maximum surface coverage of adsorbed redox species
S	Area of the electrode
E_f	Formal potential

$k_{f/b}$	Forward and backward rate constants
$I^* = I/(FcDr)$	Dimensionless current
$I_{ss}^* = I_{ss}/(FcDr)$	Dimensionless steady-state current
$\eta^* = \eta F/(RT)$	Dimensionless overpotential
$\lambda^* = \lambda F/(RT)$	Dimensionless reorganization energy
$\varepsilon^* = \varepsilon F/(RT)$	Dimensionless energy level
$k_0^* = k_0 r/D$	Dimensionless electron-transfer rate constant
$k_c^* = k_c c r^2/D$ or $k_c^* = k_c \Gamma_{max} r/D$	Dimensionless second-order rate constant of the EC' reaction

Reference

•of special interest; ••of outstanding interest.

1. Mirkin, M. V.; Sun, T.; Yu, Y.; Zhou, M., Electrochemistry at One Nanoparticle. Acc. Chem. Res. 2016, 49, 2328-2335.

2. Cheng, W.; Compton, R. G., Electrochemical Detection of Nanoparticles by 'Nano-Impact' Methods. TrAC, Trends Anal. Chem. 2014, 58, 79-89.

• 3. Sokolov, S. V.; Eloul, S.; Kätelhön, E.; Batchelor-McAuley, C.; Compton, R. G., Electrode-Particle Impacts: A Users Guide. Phys. Chem. Chem. Phys. 2017, 19, 28-43.

This work is a practical and comprehensive tutorial on both fundamental aspects and applications of the nano-impact technique.

4. Stevenson, K. J.; Tschulik, K., A Materials Driven Approach for Understanding Single Entity Nano Impact Electrochemistry. Current Opinion in Electrochemistry 2017, 6, 38-45.

5. Allerston, L. K.; Rees, N. V., Nanoparticle Impacts in Innovative Electrochemistry. Current Opinion in Electrochemistry 2018.

6. Chen, S.; Liu, Y., Electrochemistry at Nanometer-Sized Electrodes. Phys. Chem. Chem. Phys. 2014, 16, 635-652.

7. Compton, R. G.; Laborda, E.; Ward, K. R., Understanding Voltammetry: Simulation of Electrode Processes; Imperial College Press: London, U.K., 2013.

8. Britz, D. H.; Strutwolf, J., Digital Simulation in Electrochemistry : Fourth Edition., 4th Ed ed.; Springer, 2016.

9. Dickinson, E. J. F.; Ekström, H.; Fontes, E., Comsol Multiphysics®: Finite Element Software for Electrochemical Analysis. A Mini-Review. Electrochem. Commun. 2014, 40, 71-74.

10. Kahk, J. M.; Rees, N. V.; Pillay, J.; Tshikhudo, R.; Vilakazi, S.; Compton, R. G., Electron Transfer Kinetics at Single Nanoparticles. Nano Today 2012, 7, 174-179.

11. Ward, K. R.; Lawrence, N. S.; Seth Hartshorne, R.; Compton, R. G., Modelling the Steady State Voltammetry of a Single Spherical Nanoparticle on a Surface. J. Electroanal. Chem. 2012, 683, 37-42.

12. Feldberg, S. W., Implications of Marcus-Hush Theory for Steady-State Heterogeneous Electron Transfer at an Inlaid Disk Electrode. Anal. Chem. 2010, 82, 5176-5183.

13. Henstridge, M. C.; Ward, K. R.; Compton, R. G., The Marcus-Hush Model of Electrode Kinetics at a Single Nanoparticle. J. Electroanal. Chem. 2014, 712, 14-18.

14. Laborda, E.; Henstridge, M. C.; Compton, R. G., Asymmetric Marcus Theory: Application to Electrode Kinetics. J. Electroanal. Chem. 2012, 667, 48-53.

15. Henstridge, M. C.; Laborda, E.; Wang, Y.; Suwatchara, D.; Rees, N.; Molina, Á.; Martínez-Ortiz, F.; Compton, R. G., Giving Physical Insight into the Butler–Volmer Model of Electrode Kinetics: Application of Asymmetric Marcus–Hush Theory to the Study of the Electroreductions of 2-Methyl-2-Nitropropane, Cyclooctatetraene and Europium(Iii) on Mercury Microelectrodes. J. Electroanal. Chem. 2012, 672, 45-52.

16. Henstridge, M. C.; Laborda, E.; Compton, R. G., Asymmetric Marcus–Hush Model of Electron Transfer Kinetics: Application to the Voltammetry of Surface-Bound Redox Systems. J. Electroanal. Chem. 2012, 674, 90-96.

17. Agyekum, I.; Nimley, C.; Yang, C.; Sun, P., Combination of Scanning Electron Microscopy in the Characterization of a Nanometer-Sized Electrode and Current Fluctuation Observed at a Nanometer-Sized Electrode. The Journal of Physical Chemistry C 2010, 114, 14970-14974.

18. Hoeben, F. J. M.; Meijer, F. S.; Dekker, C.; Albracht, S. P. J.; Heering, H. A.; Lemay, S. G., Toward Single-Enzyme Molecule Electrochemistry: [Nife]-Hydrogenase Protein Film Voltammetry at Nanoelectrodes. ACS Nano 2008, 2, 2497-2504.

19. Streeter, I.; Compton, R. G., Diffusion-Limited Currents to Nanoparticles of Various Shapes Supported on an Electrode; Spheres, Hemispheres, and Distorted Spheres and Hemispheres. The Journal of Physical Chemistry C 2007, 111, 18049-18054.

20. Ying, Y.; Ding, Z.; Zhan, D.; Long, Y., Advanced Electroanalytical Chemistry at Nanoelectrodes. Chem. Sci. 2017, 8, 3338-3348.

21. Hua, H.; Liu, Y.; Guan, X.; Li, Y., DNA Nanosensors Based on the Use of Single Gold Nanowire Electrodes and Methylene Blue as an Intercalator. Microchimica Acta 2018, 185.

22. Aoki, K., Theory of Ultramicroelectrodes. Electroanalysis 1993, 5, 627-639.

23. Kim, J.; Bard, A. J., Electrodeposition of Single Nanometer-Size Pt Nanoparticles at a Tunneling Ultramicroelectrode and Determination of Fast Heterogeneous Kinetics for Ru(Nh3)63+ Reduction. J. Am. Chem. Soc. 2016, 138, 975-979.

24. Dawson, K.; Wahl, A.; Murphy, R.; O'Riordan, A., Electroanalysis at Single Gold Nanowire Electrodes. The Journal of Physical Chemistry C 2012, 116, 14665-14673.

25. Heller, I.; Kong, J.; Heering, H. A.; Williams, K. A.; Lemay, S. G.; Dekker, C., Individual Single-Walled Carbon Nanotubes as Nanoelectrodes for Electrochemistry. Nano Lett. 2005, 5, 137-142.

• 26. Zhang, B.; Fan, L.; Zhong, H.; Liu, Y.; Chen, S., Graphene Nanoelectrodes: Fabrication and Size-Dependent Electrochemistry. J. Am. Chem. Soc. 2013, 135, 10073-10080.

The electroactivity of nanosized graphenes is measured on single graphene particles with various sizes. In combination with Raman spectroscopic result, structure-dependent electroactivity was studied. The design of the electrode system makes it possible to measure a whole polarization curve and therefore the electron-transfer rate constant as well as the size of the graphene simultaneously.

27. Dudin, P. V.; Snowden, M. E.; Macpherson, J. V.; Unwin, P. R., Electrochemistry at Nanoscale Electrodes: Individual Single-Walled Carbon Nanotubes (Swnts) and Swnt-Templated Metal Nanowires. ACS Nano 2011, 5, 10017-10025.

28. Percival, S. J.; Zhang, B., Fast-Scan Cyclic Voltammetry Allows Determination of Electron-Transfer Kinetic Constants in Single Nanoparticle Collision. The Journal of Physical Chemistry C 2016, 120, 20536-20546.

29. Chen, S.; Liu, Y.; Chen, J., Heterogeneous Electron Transfer at Nanoscopic Electrodes: Importance of Electronic Structures and Electric Double Layers. Chem. Soc. Rev. 2014, 43, 5372-5386.

•• 30. Dickinson, E. J. F.; Compton, R. G., Influence of the Diffuse Double Layer on Steady-State Voltammetry. J. Electroanal. Chem. 2011, 661, 198-212.

This work provides a fully comprehensive discussion on the theory and modelling of the diffuse double layer. The steady-state voltammetric current responses under the influence of the species charge, the electrolyte concentration, the electron-transfer kinetics, the electron tunnelling and the ion activity are presented in detail.

31. He, R.; Chen, S.; Yang, F.; Wu, B., Dynamic Diffuse Double-Layer Model for the Electrochemistry of Nanometer-Sized Electrodes. The Journal of Physical Chemistry B 2006, 110, 3262-3270.

32. Edwards, P. P.; Gray, H. B.; Lodge, M. T. J.; Williams, R. J. P., Electron Transfer and Electronic Conduction through an Intervening Medium. Angew. Chem. Int. Ed. 2008, 47, 6758-6765.

33. Liu, Y.; He, R.; Zhang, Q.; Chen, S., Theory of Electrochemistry for Nanometer-Sized Disk Electrodes. The Journal of Physical Chemistry C 2010, 114, 10812-10822.

34. Bae, J. H.; Yu, Y.; Mirkin, M. V., Diffuse Layer Effect on Electron-Transfer Kinetics Measured by Scanning Electrochemical Microscopy (Secm). The Journal of Physical Chemistry Letters 2017, 8, 1338-1342.

35. Streeter, I.; Baron, R.; Compton, R. G., Voltammetry at Nanoparticle and Microparticle Modified Electrodes: Theory and Experiment. The Journal of Physical Chemistry C 2007, 111, 17008-17014.

36. Henstridge, M. C.; Compton, R. G., Mass Transport to Micro- and Nanoelectrodes and Their Arrays: A Review. The Chemical Record 2012, 12, 63-71.

37. Godino, N.; Borrisé, X.; Muñoz, F. X.; del Campo, F. J.; Compton, R. G., Mass Transport to Nanoelectrode Arrays and Limitations of the Diffusion Domain Approach: Theory and Experiment. The Journal of Physical Chemistry C 2009, 113, 11119-11125.

•• 38. Costentin, C.; Di Giovanni, C.; Giraud, M.; Savéant, J.-M.; Tard, C., Nanodiffusion in Electrocatalytic Films. Nature Materials 2017, 16, 1016.

This work demonstrates the competition between nanodiffusion and linear diffusion for catalytic nanoparticle modified electrodes. A simple and clear competition parameter is applied in the model, including all the operational and structural experimental conditions. The model is tested by comparing with the experiment of the hydrogen evolution reaction on a mixture of platinum nanoparticles with carbon dispersed in a Nafion film.

39. Gara, M.; Ward, K. R.; Compton, R. G., Nanomaterial Modified Electrodes: Evaluating Oxygen Reduction Catalysts. Nanoscale 2013, 5, 7304-7311.

40. Streeter, I.; Wildgoose, G. G.; Shao, L.; Compton, R. G., Cyclic Voltammetry on Electrode Surfaces Covered with Porous Layers: An Analysis of Electron Transfer Kinetics at Single-Walled Carbon Nanotube Modified Electrodes. Sensors Actuators B: Chem. 2008, 133, 462-466.

41. Akinoglu, E. M.; Kätelhön, E.; Pampel, J.; Ban, Z.; Antonietti, M.; Compton, R. G.; Giersig, M., Nanoscopic Carbon Electrodes: Structure, Electrical Properties and Application for Electrochemistry. Carbon 2018, 130, 768-774.

42. Sims, M. J.; Rees, N. V.; Dickinson, E. J. F.; Compton, R. G., Effects of Thin-Layer Diffusion in the Electrochemical Detection of Nicotine on Basal Plane Pyrolytic Graphite (Bppg) Electrodes Modified with Layers of Multi-Walled Carbon Nanotubes (Mwcnt-Bppg). Sensors Actuators B: Chem. 2010, 144, 153-158.

43. Ward, K. R.; Compton, R. G., Quantifying the Apparent 'Catalytic' Effect of Porous Electrode Surfaces. J. Electroanal. Chem. 2014, 724, 43-47.

44. Brookes, B. A.; Davies, T. J.; Fisher, A. C.; Evans, R. G.; Wilkins, S. J.; Yunus, K.; Wadhawan, J. D.; Compton, R. G., Computational and Experimental Study of the Cyclic Voltammetry Response of Partially Blocked Electrodes. Part 1. Nonoverlapping, Uniformly Distributed Blocking Systems. The Journal of Physical Chemistry B 2003, 107, 1616-1627.

45. Menshykau, D.; Compton, R. G., The Influence of Electrode Porosity on Diffusional Cyclic Voltammetry. Electroanalysis 2008, 20, 2387-2394.

46. Menshykau, D.; Compton, R. G., Electrodes Modified with Electroinactive Layers: Distinguishing through-Film Transport from Pinhole (Pore) Diffusion. Langmuir 2009, 25, 2519-2529.

47. Eloul, S.; Compton, R. G., Voltammetric Sensitivity Enhancement by Using Preconcentration Adjacent to the Electrode: Simulation, Critical Evaluation, and Insights. The Journal of Physical Chemistry C 2014, 118, 24520-24532.

48. Chan, H. T. H.; Kätelhön, E.; Compton, R. G., Voltammetry at Electrodes Decorated with an Insulating Porous Film: Understanding the Effects of Adsorption. J. Electroanal. Chem. 2017, 801, 135-140.

49. Huang, J.; Zhang, J.; Eikerling, M. H., Particle Proximity Effect in Nanoparticle Electrocatalysis: Surface Charging and Electrostatic Interactions. The Journal of Physical Chemistry C 2017, 121, 4806-4815.

50. Speder, J.; Altmann, L.; Bäumer, M.; Kirkensgaard, J. J. K.; Mortensen, K.; Arenz, M., The Particle Proximity Effect: From Model to High Surface Area Fuel Cell Catalysts. RSC Advances 2014, 4, 14971-14978.

51. Molina, A.; González, J.; Laborda, E.; Compton, R. G., Analytical Theoretical Approach to the Transient and Steady State Voltammetric Response of Reaction Mechanisms. Linear Diffusion and Reaction Layers at Micro- and Submicroelectrodes of Arbitrary Geometry. J. Electroanal. Chem. 2016, 782, 59-66.

• 52. Bieniasz, L. K.; González, J.; Molina, Á.; Laborda, E., Theory of Linear Sweep/Cyclic Voltammetry for the Electrochemical Reaction Mechanism Involving a Redox Catalyst Couple Attached to a Spherical Electrode. Electrochim. Acta 2010, 56, 543-552.

The analytical expression of the voltammetric features is derived for the EC' reaction in this work, providing a general, comprehensive theoretical view. The results are helpful in the analysis of experimental data.

53. Savéant, J.-M., Molecular Catalysis of Electrochemical Reactions. Mechanistic Aspects. Chem. Rev. 2008, 108, 2348-2378.

54. Lin, C.; Compton, R. G., Size Effects in Nanoparticle Catalysis at Nanoparticle Modified Electrodes: The Interplay of Diffusion and Chemical Reactions. The Journal of Physical Chemistry C 2017, 121, 2521-2528.

55. Lin, Q.; Lin, C.; Wu, H.; Batchelor-McAuley, C.; Compton, R. G., Catalytic Single-Particle Nano-Impacts: Theory and Experiment. Poly(Vinylferrocene)-Modified Graphene Nanoplatelet Mediated L-Cysteine Oxidation. The Journal of Physical Chemistry C 2016, 120, 20216-20223.

• 56. Molina, Á.; Laborda, E.; Gómez-Gil, J. M.; Martínez-Ortiz, F.; Compton, R. G., A Comprehensive Voltammetric Characterisation of Ece Processes. Electrochim. Acta 2016, 195, 230-245.

This work provides a generic approach for the determination of the electrocatalytic nanoeffect, where the influence of mass transport is taken into consideration.

57. Ward, K. R.; Gara, M.; Lawrence, N. S.; Hartshorne, R. S.; Compton, R. G., Nanoparticle Modified Electrodes Can Show an Apparent Increase in Electrode Kinetics Due Solely to Altered Surface Geometry: The Effective Electrochemical Rate Constant for Non-Flat and Non-Uniform Electrode Surfaces. J. Electroanal. Chem. 2013, 695, 1-9.

58. Wang, Y.; Ward, K. R.; Laborda, E.; Salter, C.; Crossley, A.; Jacobs, R. M. J.; Compton, R. G., A Joint Experimental and Computational Search for Authentic Nano‐Electrocatalytic Effects: Electrooxidation of Nitrite and L‐Ascorbate on Gold Nanoparticle‐Modified Glassy Carbon Electrodes. Small 2013, 9, 478-486.

59. Chen, S.; Kucernak, A., Electrocatalysis under Conditions of High Mass Transport: Investigation of Hydrogen Oxidation on Single Submicron Pt Particles Supported on Carbon. The Journal of Physical Chemistry B 2004, 108, 13984-13994.

60. Jiao, X.; Lin, C.; Young, N. P.; Batchelor-McAuley, C.; Compton, R. G., Hydrogen Oxidation Reaction on Platinum Nanoparticles: Understanding the Kinetics of Electrocatalytic Reactions Via "Nano-Impacts". The Journal of Physical Chemistry C 2016, 120, 13148-13158.

61. Zhou, Y.; Rees, N. V.; Compton, R. G., Electrochemistry of Nickel Nanoparticles Is Controlled by Surface Oxide Layers. Phys. Chem. Chem. Phys. 2013, 15, 761-763.

62. Wang, Y.; Laborda, E.; Tschulik, K.; Damm, C.; Molina, A.; Compton, R. G., Strong Negative Nanocatalysis: Oxygen Reduction and Hydrogen Evolution at Very Small (2 Nm) Gold Nanoparticles. Nanoscale 2014, 6, 11024-11030.

63. Xiang, Z.; Deng, H.; Peljo, P.; Fu, Z.; Wang, S.; Mandler, D.; Sun, G.; Liang, Z., Electrochemical Dynamics of a Single Platinum Nanoparticle Collision Event for the Hydrogen Evolution Reaction. Angew. Chem. Int. Ed. 2018, 57, 3464-3468.

64. Wroblowa, H. S.; Yen Chi, P.; Razumney, G., Electroreduction of Oxygen: A New Mechanistic Criterion. Journal of Electroanalytical Chemistry and Interfacial Electrochemistry 1976, 69, 195-201.

•• 65. Chen, S.; Kucernak, A., Electrocatalysis under Conditions of High Mass Transport Rate: Oxygen Reduction on Single Submicrometer-Sized Pt Particles Supported on Carbon. The Journal of Physical Chemistry B 2004, 108, 3262-3276.

The theoretical model clearly explains the variation of oxygen reduction reaction from 4e- transfer to 2e- transfer when decreasing the electrode size. This paper provides important guidance in understanding the kinetics of the oxygen reduction reaction on nanoparticles and nanoelectrodes.

66. Yang, H.; Kumar, S.; Zou, S., Electroreduction of O2 on Uniform Arrays of Pt Nanoparticles. J. Electroanal. Chem. 2013, 688, 180-188.

67. Gara, M.; Laborda, E.; Holdway, P.; Crossley, A.; Jones, C. J. V.; Compton, R. G., Oxygen Reduction at Sparse Arrays of Platinum Nanoparticles in Aqueous Acid: Hydrogen Peroxide as a Liberated Two Electron Intermediate. Phys. Chem. Chem. Phys. 2013, 15, 19487-19495.

68. Wang, Y.; Laborda, E.; Ward, K. R.; Tschulik, K.; Compton, R. G., A Kinetic Study of Oxygen Reduction Reaction and Characterization on Electrodeposited Gold Nanoparticles of Diameter between 17 Nm and 40 Nm in 0.5 M Sulfuric Acid. Nanoscale 2013, 5, 9699-9708.

69. Wang, Y.; Laborda, E.; Plowman, B. J.; Tschulik, K.; Ward, K. R.; Palgrave, R. G.; Damm, C.; Compton, R. G., The Strong Catalytic Effect of Pb(Ii) on the Oxygen Reduction Reaction on 5 Nm Gold Nanoparticles. Phys. Chem. Chem. Phys. 2014, 16, 3200-3208.

70. Qiao, J.; Liu, Y.; Hong, F.; Zhang, J., A Review of Catalysts for the Electroreduction of Carbon Dioxide to Produce Low-Carbon Fuels. Chem. Soc. Rev. 2014, 43, 631-675.

71. Wang, Y.; Liu, J.; Wang, Y.; Al‐Enizi, A. M.; Zheng, G., Tuning of Co2 Reduction Selectivity on Metal Electrocatalysts. Small 2017, 13, 1701809.

• 72. Costentin, C.; Savéant, J.-M., Catalysis at the Nanoscale May Change Selectivity. Proceedings of the National Academy of Sciences 2016, 113, 11756-11758.

The product selectivity from macroscale to nanoscale is modelled. In the carbon dioxide reduction coupled with the hydrogen evolution reaction, the producing formate is predicted as a function of the diffusion layer thickness, showing the effect of nanoscaling on product selectivity.

73. Mistry, H.; Behafarid, F.; Reske, R.; Varela, A. S.; Strasser, P.; Roldan Cuenya, B., Tuning Catalytic Selectivity at the Mesoscale Via Interparticle Interactions. ACS Catal. 2016, 6, 1075-1080.

•• 74. Liu, M., et al., Enhanced Electrocatalytic CO_2 Reduction Via Field-Induced Reagent Concentration. Nature 2016, 537, 382.

The tip-enhanced field phenomenon on the CO_2 electroreduction is reported and explained by a combined experimental and theoretical study. It is found that the local high electric fields on the tip concentrate electrolyte cations and the electrolyte cations can reduce the reaction barrier of the CO_2 reduction, providing useful suggestions on designing effective electrocatalysts.

• 75. Jiang, H.; Hou, Z.; Luo, Y., Unraveling the Mechanism for the Sharp-Tip Enhanced Electrocatalytic Carbon Dioxide Reduction: The Kinetics Decide. Angew. Chem. Int. Ed. 2017, 56, 15617-15621.

This work demonstrates that the kinetic factors, the mass transport and the surface adsorption rate of carbon dioxide, are rate-determining steps in the carbon dioxide reduction enhanced by the sharp-tip nano-electrocatalyst. The significance of kinetic simulation is emphasized.

76. Oldham, K. B.; Myland, J. C., Modelling Cyclic Voltammetry without Digital Simulation. Electrochim. Acta 2011, 56, 10612-10625.

77. Cutress, I. J.; Dickinson, E. J. F.; Compton, R. G., Analysis of Commercial General Engineering Finite Element Software in Electrochemical Simulations. J. Electroanal. Chem. 2010, 638, 76-83.

•• 78. Molina, Á.; González, J., Pulse Voltammetry in Physical Electrochemistry and Electroanalysis: Theory and Applications; Springer International Publishing, 2015.

A complete theoretical description including exceptionally clear mathematical derivations of various pulse voltammetry techniques is presented in this book.

79. Novev, J. K.; Compton, R. G., Natural Convection Effects in Electrochemical Systems. Current Opinion in Electrochemistry 2018, 7, 118-129.

80. Rudolph, M.; Reddy, D. P.; Feldberg, S. W., A Simulator for Cyclic Voltammetric Responses. Anal. Chem. 1994, 66, 589A-600A.

81. Semenova, D.; Zubov, A.; Silina, Y. E.; Micheli, L.; Koch, M.; Fernandes, A. C.; Gernaey, K. V., Mechanistic Modeling of Cyclic Voltammetry: A Helpful Tool for Understanding Biosensor Principles and Supporting Design Optimization. Sensors and Actuators, B: Chemical 2018, 259, 945-955.

82. Kuss, S.; Tanner, E. E. L.; Ordovas-Montanes, M.; Compton, R. G., Electrochemical Recognition and Quantification of Cytochrome C Expression In: Bacillus Subtilis and Aerobe/Anaerobe Escherichia Coli Using N, N, N′, N′-Tetramethyl- Para -Phenylene-Diamine (Tmpd). Chem. Sci. 2017, 8, 7682-7688.

• 83. Klymenko, O. V.; Svir, I.; Amatore, C., New Theoretical Insights into the Competitive Roles of Electron Transfers Involving Adsorbed and Homogeneous Phases. J. Electroanal. Chem. 2013, 688, 320-327.

This paper shows an authoritative account of simulating the adsorption-involved electrochemical reactions, especially the competition between different adsorbates. A clear model was developed and simulation details were provided.

84. Pérez-Brokate, C. F.; di Caprio, D.; Mahé, É.; Féron, D.; de Lamare, J., Cyclic Voltammetry Simulations with Cellular Automata. Journal of Computational Science 2015, 11, 269-278.

85. Kätelhön, E.; Tanner, E. E. L.; Batchelor-McAuley, C.; Compton, R. G., Destructive Nano-Impacts: What Information Can Be Extracted from Spike Shapes? Electrochim. Acta 2016, 199, 297-304.

86. Jiao, X.; Batchelor-McAuley, C.; Lin, C.; Kätelhön, E.; Tanner, E. E. L.; Young, N. P.; Compton, R. G., Role of Nanomorphology and Interfacial Structure of Platinum Nanoparticles in Catalyzing the Hydrogen Oxidation Reaction. ACS Catal. 2018, 8, 6192-6202.